ELSEVIER

Engineering Geology 53 (1998) 195–204

ENGINEERING GEOLOGY

Pollution transport studies using an in-situ fibre optic photometric sensor

A.C.J. Treadaway, R.J. Lynch, M.D. Bolton *

Cambridge University Engineering Department, Cambridge, UK.

Abstract

In order to study the migration of contaminants in soils, we are currently using an in situ fibre optic sensor to track the movement of a dye tracer. Details of the sensor is discussed and the results presented of one-dimensional transport experiments using a water soluble dye and a copper salt. Water was forced to percolate downwards in a bed of fine sand, with the hydraulic gradient kept constant during any given experiment. A pulse of contaminant was released on the soil surface, and its concentration was subsequently measured using sensors buried at two depths. This permitted the pollution plume to be tracked. It was found that the width was independent of hydraulic gradient, as predicted by the theory of mechanical dispersion for seepage flows with a high Peclet number. © 1999 Published by Elsevier Science B.V. All rights reserved.

Keywords: Dye tracer; Fibre optic sensor; Pollution transport

1. Introduction

The transport of pollutants through soils is a topic of increasing interest. There are two alternative approaches for the study of a pollutant plume as it moves through a bed of soil. One possibility is to take samples periodically in a three-dimensional distribution around the source of the pollution and to analyse these chemically for the pollutant of interest. A more elegant approach is to study the pollutant in-situ using a sensor. Unfortunately relatively few in-situ pollution detectors have been available. In our laboratory we are developing sensors capable of studying the transport of pollutants; one such method is by photometric detection. Optical fibres were used to measure the absorbance of a beam of light transmitted through a small buried chamber through which the pore fluid permeates.

2. Experimental details

2.1. The photometric sensor

The photometric sensor is extremely simple, a block diagram is shown in Fig. 1. Light from a light emitting diode (LED) is coupled to a low cost 1 mm diameter optical fibre, which leads the light into the sensor body. An identical fibre occupies the opposite side of the sensor. The interior of the sensor body is an absorbance chamber through which the pore fluid of the soil passes. A porous plastic membrane prevents soil particles from blocking the light beam whilst allowing pore

* Corresponding author. Tel: +44 1223 332714; fax: +44 1223 339713.
E-mail address: rjl1@eng.cam.ac.uk (M.D. Bolton)

PII: S0013-7952(99)00033-2

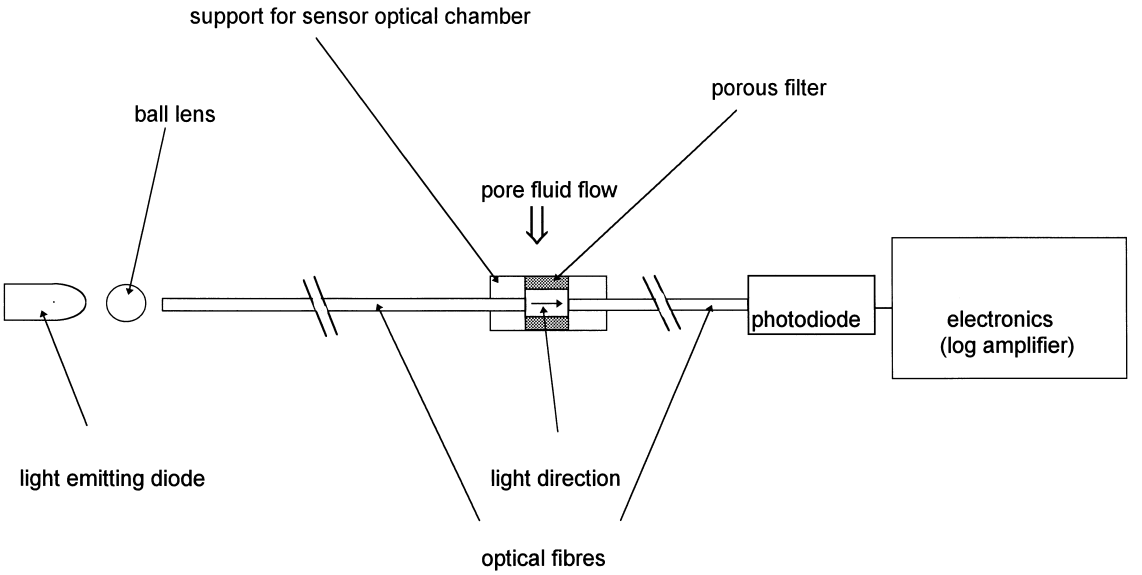

Fig. 1. Block diagram of a photometric sensor.

fluid to pass through. The wavelength of light is chosen to match the maximum absorbance of the pollutant. In this case we have selected an amber LED which emits light at 620 nm and a green dye tracer which absorbs light at this wavelength. The receiving optical fibre is coupled to a silicon photodiode which is part of a photodetection system. A logging circuit ensures that the voltage which is output from the detector is a log function of the light intensity detected by the photodiode. By the Beer–Lambert Law (for example Straughan and Walker (1976)) the light absorbed, A, by the dye, is:

$$A = \log I_o/I = \epsilon Cl, \quad (1)$$

where I_o is the pre-sensor light intensity and I is the post-sensor light intensity. This absorbance, A, is a linear function of its concentration, C, and the path length, l, where ϵ is the extinction coefficient which is constant at a given wavelength. Rearranging the above expression:

$$\log I = -\epsilon Cl + \log I_o. \quad (2)$$

The electronics are arranged to produce an output voltage which is a log function of the light intensity reaching the detector, so that the output varies linearly with dye concentration. The signal from the detection system is digitised and stored using a Handyscope 12 bit data acquisition system (from TiePie Engineering, Leeuwarden, The Netherlands) which is resident in a 486 personal computer. These sensors are calibrated by testing with known concentrations of pollutant. The sensor output (volts) versus concentration graphs are linear for both sensors with regression coefficients of around 0.998. The calibration graph for sensor 1 is shown in Fig. 2.

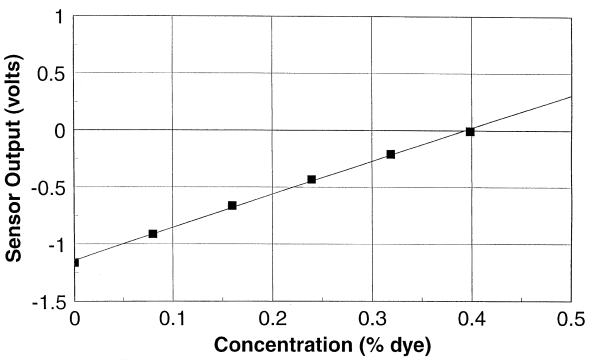

Fig. 2. Typical green dye calibration (sensor 1).

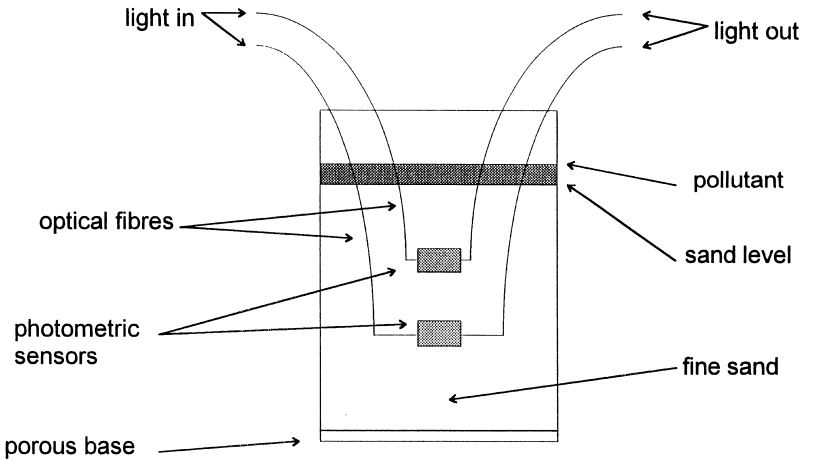

Fig. 3. Experimental arrangement.

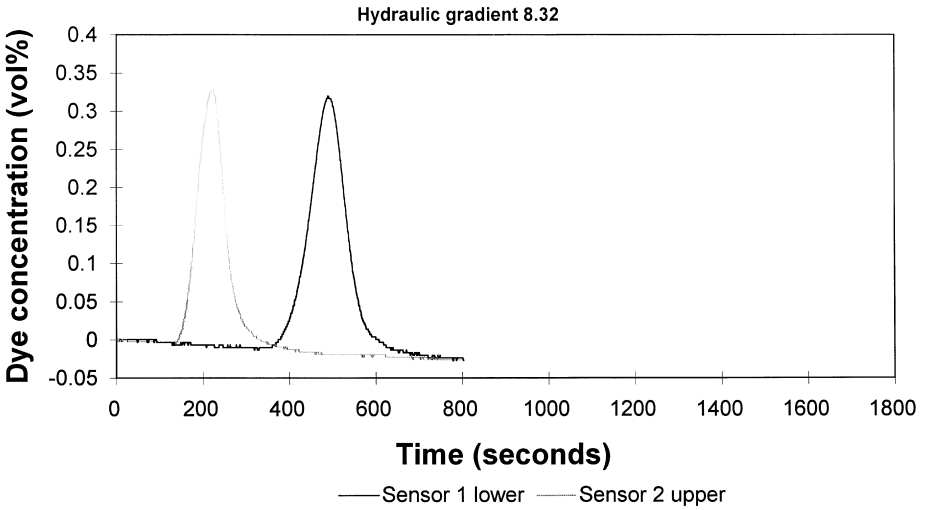

Fig. 4. Two sensor tests: dye concentration against time at a hydraulic gradient of 8.32.

2.2. Experimental tracking of green dye through fine sand

In this experiment a green food dye pollutant is applied to a soil sample and its one-dimensional progress through the soil is monitored by two sensors which are buried at about 30 mm and 80 mm below the surface. A schematic diagram of the experimental arrangement is shown in Fig. 3. A 96 mm deep homogeneous bed of 52/100 grade (300–150 μm) sand is held in a Perspex tube retained by porous plastic at the base. The sensors were buried in the saturated sand during the construction of the bed which was prepared with de-aired water. It is important to prevent air bubbles from getting into the sand bed or the sensors as they restrict the pore water flow. A hydraulic gradient is maintained across the sand and, apart from the application of the pollutant to the soil surface, it is kept constant throughout the experiment. At the start of the experiment the water height is allowed to fall almost to the sand level. Fifty millilitres of green dye pollutant is then applied to the sand, the surface of which is pro-

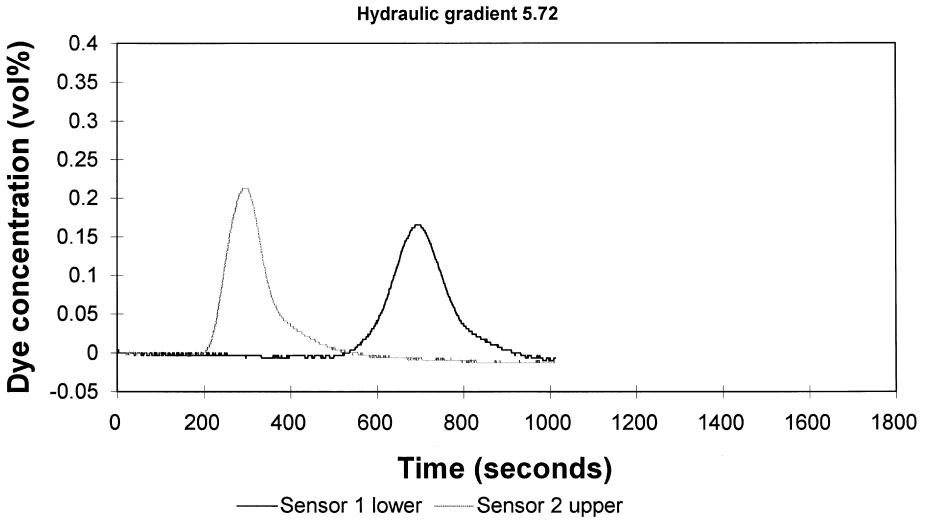

Fig. 5. Two sensor tests: dye concentration against time at a hydraulic gradient of 5.72.

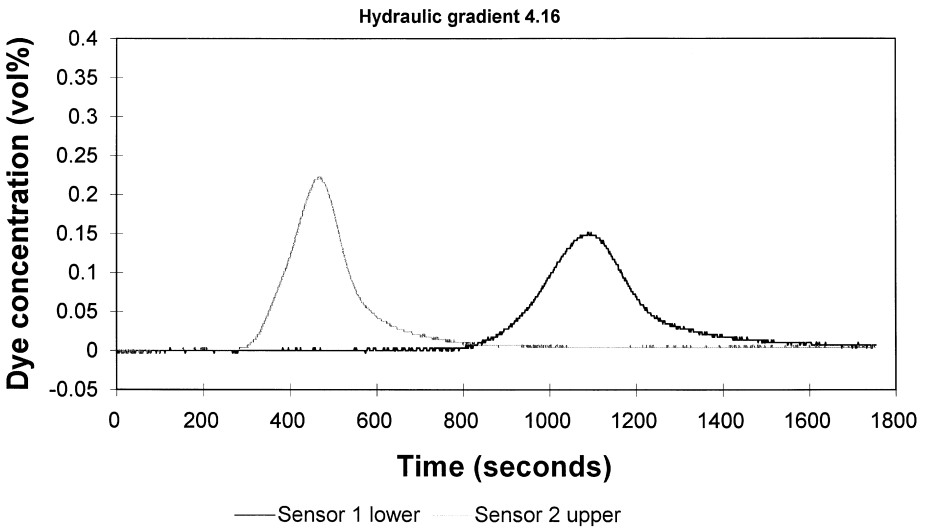

Fig. 6. Two sensor tests: dye concentration against time at a hydraulic gradient of 4.16.

tected by filter paper to prevent the sudden application of the pollutant from disturbing it. When the pollutant has almost disappeared into the sand the water level is returned to its original height and maintained there until the dye has passed out of the bed. This experiment is conducted at a number of different flow rates. The hydraulic gradient and the flow rate are varied by raising or lowering the drainage outlet.

3. Results of the tests with green dye

3.1. Series 1: two-sensor tests

Figs. 4–6 show the one-dimensional progress of the pollution plume, through a homogeneous bed of sand, picked up by the two sensors at three different hydraulic gradients. These concentration–time graphs have been produced by applying the

calibration data for each sensor to the voltage–time plots gained directly from the experiment.

It is observed, as expected, that the plumes shown by the lower sensor (sensor 1) are shorter, broader and arrive after the ones depicted by the upper sensor (sensor 2). This is because the plume has had to travel through the increased depth of sand to reach the lower sensor and has dispersed to a greater extent in the process. The plumes may be quantified by measuring: height (h), interval at half height ($\Delta t_{1/2}$), and advection time (t_{peak}). It may be noted that the $\Delta t_{1/2}$ and t_{peak} values are greater when the hydraulic gradient is smaller; this requires further discussion.

3.2. Series 2: single sensor tests

The upper sensor was then removed and green dye run through the same bed of sand at the same hydraulic gradients as in the two-sensor tests, Fig. 7 shows the results. As before the $\Delta t_{1/2}$ and t_{peak} become larger as the hydraulic gradient becomes smaller.

The original objective of these tests was to ascertain whether the presence of the upper sensor interfered with the functioning of the lower sensor. A complication which occurred was that the permeability of the sand body had decreased, either as a result of accidental air infiltration or reduction of the voids ratio following incidental compaction. This meant that even though the same hydraulic gradients were used in each set of tests, the flow rates were different. A comparison therefore relies on a more fundamental analysis of the phenomenon.

4. Interpretation

It is possible to process all these results by transforming times t into distances z using $z = v_f t$, where v_f is the mean fluid velocity in the pores. We can then assume that the plumes have a Gaussian distribution of concentration with a standard deviation, (Einstein's diffusion equation, Einstein (1905)):

$$\sigma = (2D_h t_{peak})^{1/2}, \tag{3}$$

about a mean location:

$$z = v_f t_{peak}. \tag{4}$$

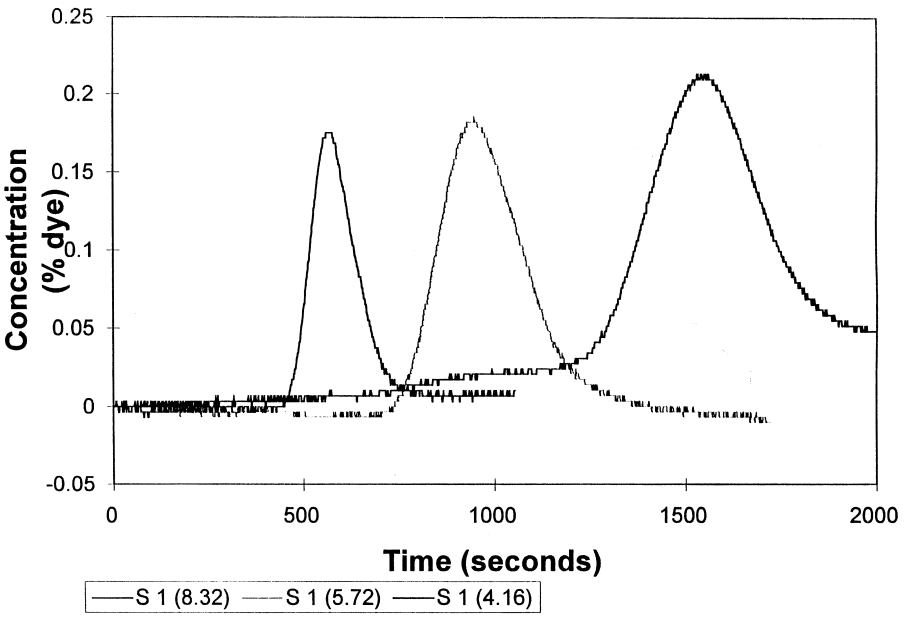

Fig. 7. One sensor tests: dye concentration against time at three different hydraulic gradients.

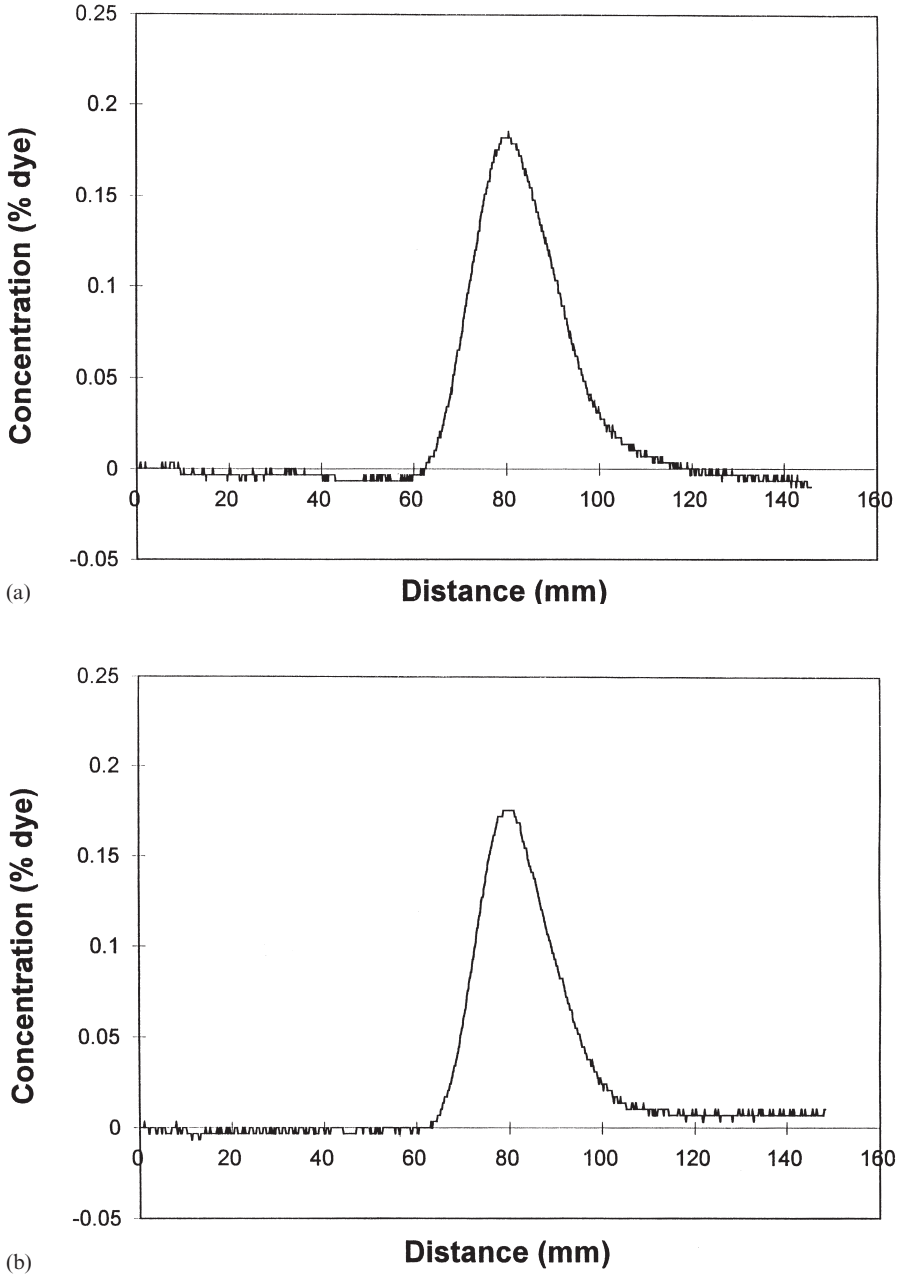

Fig. 8. One sensor tests: dye concentration against distance at a hydraulic gradient of: (a) 8.32; (b) 5.72; and (c) 4.16.

Here, D_h is the longitudinal dispersion coefficient along axis z. Dispersion is taken to comprise both molecular diffusion D_d and the extra hydrodynamic dispersion which arises from the granularity of the medium. The plumes from Fig. 7 are transformed to spatial distributions in Fig. 8(a)–(c). Apart from a small drift in the baseline concentration signal, the three plumes are almost identical. Plume width at half-height, $W_{1/2}$, is simply $v_f \Delta t_{1/2}$. Evidently $W_{1/2}$ is independent of v_f.

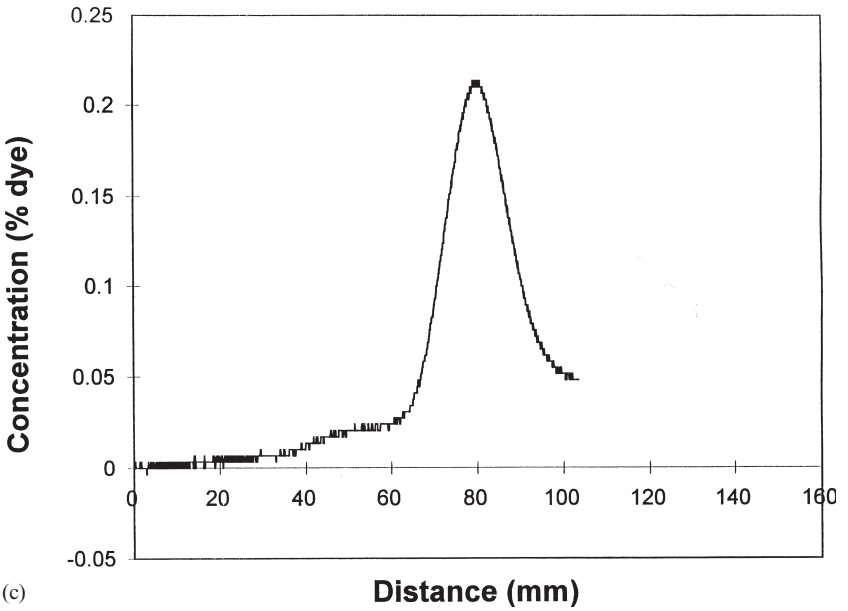

(c)

Fig. 8. (*continued*)

Tabulations of the error function show that:

$$W_{1/2} = 2.345\sigma, \tag{5}$$

which, with (3) gives:

$$D_h = \frac{(W_{1/2})^2}{11.083t}. \tag{6}$$

Taking $W_{1/2} = 18.7$ mm and $t_{peak} = 1546$ s for the plume in Fig. 8(c), for example gives $D_h = 2 \times 10^{-8}$ m^2/s. The free molecular diffusion component D_d for the green dye is thought to be of the order of 1×10^{-9} m^2/s, which would imply that hydrodynamic dispersion is the dominant mechanism. This can be confirmed using Fig. 9, which is a plot of D_h/D_d versus the Peclet number:

$$Pe = \frac{v_f d}{D_d}, \tag{7}$$

where d is the effective particle size, taken here to be $d_{10} \approx 0.2$ mm. The data from Fig. 8(a)–(c) is shown to be roughly on the line:

$$D_h = v_f d, \tag{8}$$

and to conform to other published data (Bear, 1972).

Note that previous work (Freeze and Cherry, 1979) showed that D_h/D_d has a lower cut off, equal to tortuosity T, for $Pe < 1$. Pe is greater than 10 in our current tests which confirms hydrodynamic dispersion is the significant agent. Hensley and Randolph (1994) published similar findings for sodium chloride, albeit at somewhat smaller Peclet numbers.

Taking (8) into (3) and substituting into (5) gives:

$$W_{1/2} = 2.345(2v_f dt_{peak})^{1/2}, \tag{9}$$

which can be written, using (4) as:

$$W_{1/2} = 3.33(dz)^{1/2}. \tag{10}$$

This theoretical result predicts that the plume width at each depth is independent of flow rate, as observed experimentally (see Figs. 8(a)–(c)).

All the data can now be reduced into the bar chart of Fig. 10 which shows experimental values of dispersivity, D_h/v_f, for the chronological sequence of experiments referred to above. The typical value $D_h/v_f \approx 0.2$ mm agrees with the theoretical prediction in (8). If a sensor was to represent, itself, a significant heterogeneity then sensor

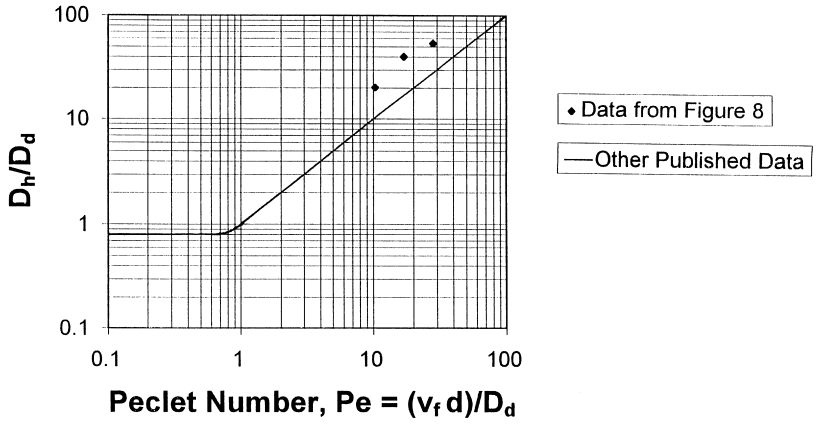

Fig. 9. Ratio of longitudinal dispersion coefficient and mean pore fluid velocity (D_h/v_f) against the Peclet number.

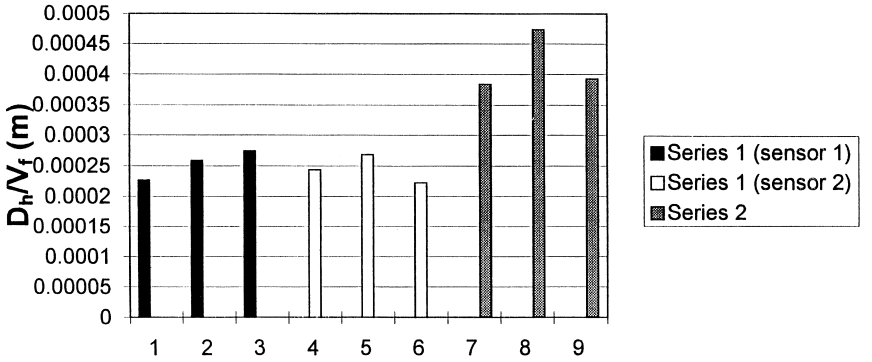

Fig. 10. Ratio of longitudinal dispersion coefficient and mean pore fluid velocity (D_f/v_f) in chronological order.

2 would have increased the dispersion recorded at sensor 1; the reverse was observed as seen in Fig. 10. Instead an increase in dispersion occurs as one experiment succeeds another; this must be related to the on going reduction of permeability which has also been mentioned. The entrapment of air bubbles would serve both to resist flow and increase heterogeneity, so this seems a likely explanation.

5. Results of tests with copper sulphate

To test the value of photometric sensors in detecting 'real' pollutants copper sulphate is used, rather than green dye, in a number of one-dimensional tests with two sensors present. In essence the experimental process was identical to the first method except that 0.1 M $CuSO_4 \cdot 5H_2O$ solution replaced the green dye. This process was carried out at various hydraulic gradients and as expected $\Delta t_{1/2}$ and t_{peak} became larger as the hydraulic gradient decreased. What was unexpected, however, was that the plume shapes were different to those of the green dye and the lower sensor in each case picked up a plume of smaller $\Delta t_{1/2}$ than the upper, see Fig.11. A possible explanation is that this was due to copper adsorption on the sand particles.

In order to substantiate the copper adsorption theory the cylinder was repacked with clean sand and a one-dimensional copper test was run, as

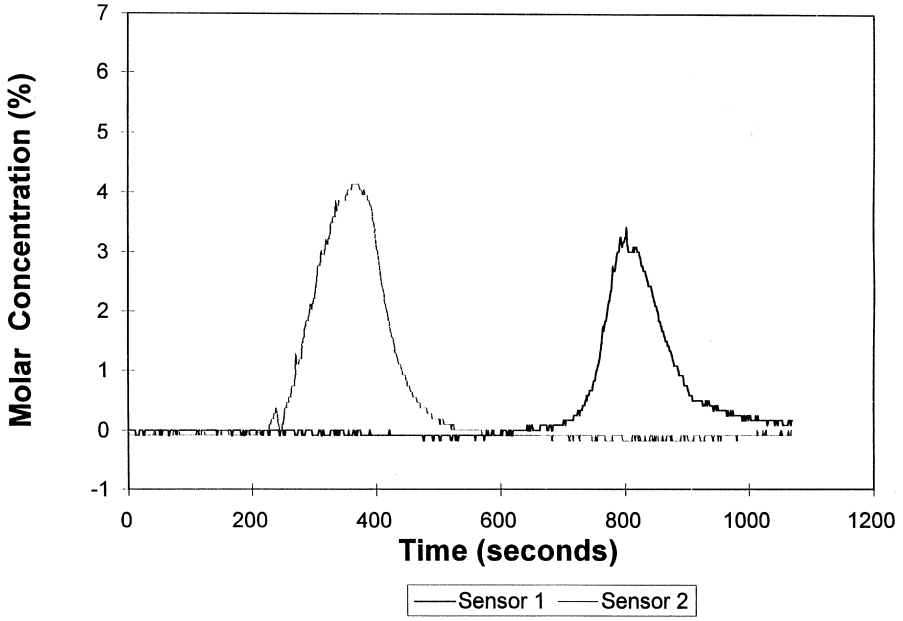

Fig. 11. Copper sulphate test: concentration against time at a hydraulic gradient of 5.72.

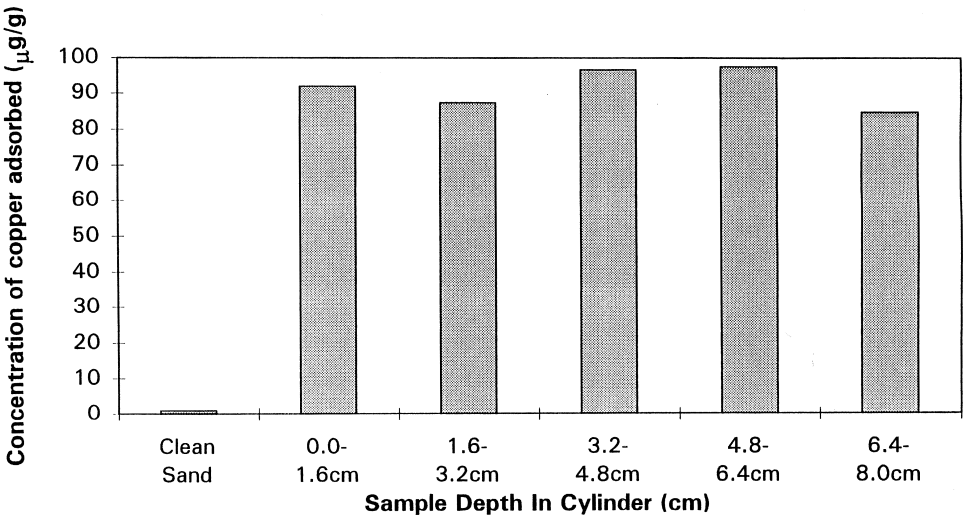

Fig. 12. Copper concentration of sand at various depths.

before. The copper solution was allowed to flow out naturally and then the bed was drained. 'Core samples' of the bed were taken and split into five sections. The five samples were dried in an oven overnight, along with a control sample of clean sand. The samples were then acid-digested and the resulting solutions tested for copper ions using an atomic absorption spectrometer. The results can be seen in Fig. 12. The clean sand contained about 1 μg of copper per gram and the used sand between 85–98 μg per gram throughout its depth. Therefore, these results are consistent with the hypothesis that sand adsorbs copper and does so more or less constantly with depth.

6. Conclusions

1. A photometric detector for measuring, in-situ, the pollutant plumes of light absorbing compounds has been designed and constructed. It has been tested by burying the sensor in beds of sand and introducing a simulated pollutant of green food dye which was released as a one-dimensional pulse. Copper sulphate plumes were also tracked. The plume size decreased with depth as a result of adsorbance of copper on the sand.
2. The sensors have been used to observe plume width and advection speed v_f, leading to computations of the local coefficient of dispersion. It has been demonstrated that dispersivity D_h/v_f is roughly equal to the effective particle size for a fast flow regime in which hydrodynamic dispersion far exceeds molecular diffusion with $Pe > 10$. This results in plume widths which are independent of advection speed and proportional to $\sqrt{(dz)}$.
3. It is thought that air bubbles became entrapped in the soil when samples were tested continuously with their top surfaces exposed intermittently to the atmosphere. This would explain the progressive reduction of permeability and increase of dispersivity which was observed.
4. In the future we intend to use UV light, rather than visible light, to extend the process to a wide range of organic pollutants.

Acknowledgements

Support from the EPSRC for A. Treadaway is gratefully acknowledged. Thanks are due to S. Chandler and T. Ablett for mechanical assistance and to T. Wilmshurst and G. Bailey for electronic support.

References

Bear, J., 1972. Dynamics of Fluids in Porous Media. American Elsevier.

Einstein, A., 1905. Ann. der Physik 17, 549

Freeze, R.A., Cherry, J.A., 1979. Groundwater. Prentice-Hall, Englewood-Cliffs, NJ.

Hensley, P.J., Randolph, M.F., 1994. Modelling contaminant dispersion in saturated sand. XIII ICSMFE (XII International Conference of Soil Mechanics and Foundation Engineering), vol. 4, pp. 1557–1560.

Straughan, B.P., Walker, S., 1976. Spectroscopy 3. Chapman & Hall, London.